Pseudopotential-based electron quantum transport: Theoretical formulation and application to nanometer-scale silicon nanowire transistors

Jingtian Fang,[a] William G. Vandenberghe, Bo Fu,[b] and Massimo V. Fischetti
Department of Materials Science and Engineering, The University of Texas at Dallas, Richardson, Texas 75080, USA

(Received 30 September 2015; accepted 4 January 2016; published online 15 January 2016)

We present a formalism to treat quantum electronic transport at the nanometer scale based on empirical pseudopotentials. This formalism offers explicit atomistic wavefunctions and an accurate band structure, enabling a detailed study of the characteristics of devices with a nanometer-scale channel and body. Assuming externally applied potentials that change slowly along the electron-transport direction, we invoke the envelope-wavefunction approximation to apply the open boundary conditions and to develop the transport equations. We construct the full-band open boundary conditions (self-energies of device contacts) from the complex band structure of the contacts. We solve the transport equations and present the expressions required to calculate the device characteristics, such as device current and charge density. We apply this formalism to study ballistic transport in a gate-all-around (GAA) silicon nanowire field-effect transistor with a body-size of 0.39 nm, a gate length of 6.52 nm, and an effective oxide thickness of 0.43 nm. Simulation results show that this device exhibits a subthreshold slope (SS) of ~66 mV/decade and a drain-induced barrier-lowering of ~2.5 mV/V. Our theoretical calculations predict that low-dimensionality channels in a 3D GAA architecture are able to meet the performance requirements of future devices in terms of SS swing and electrostatic control. © *2016 AIP Publishing LLC*. [http://dx.doi.org/10.1063/1.4939963]

I. INTRODUCTION

The complexity of studying electronic transport in a quantum-mechanical formalism while accounting for the atomistic nature of nanostructures is notoriously daunting. Several simplified models have been widely employed in the past. Commonly found in the literature are models dealing with ballistic transport using self-consistent open boundary-conditions Schrödinger/Poisson solvers based on the parabolic effective-mass approximation[1–5] or models based on empirical tight-binding models[2,4,6,7] coupled to the non-equilibrium Green's function (NEGF) formalism.[8] A few studies based on pseudopotentials[5,9–12] have also been proposed. The NEGF method has been employed occasionally in simple cases to calculate scattering rates and to study dissipative transport in devices.[1,13,14] However, each of these approaches comes with its own limitations.

The parabolic effective-mass approximation has been used to simulate ballistic and dissipative quantum transport in silicon nanowire (SiNW) field-effect transistors (FETs) with a 10 nm gate-length and a 3 nm silicon body thickness.[1] However, the effective-mass approximation loses its ability to accurately describe the electronic band structure and predict the device characteristics for silicon bodies thinner than about 3 nm, due to the strong nonparabolicity of the energy bands at this ultra-confined scale.[2,4,7] Furthermore, the effective-mass approximation method cannot resolve the atomistic features of devices, which are important when devices are scaled down to nanometer dimensions.[15]

For these reasons, a full-band empirical tight-binding approach using a small atomic orbital basis (5–10 orbitals per atom, such as sp^3s^* or $sp^3d^5s^*$) within the NEGF transport model has been widely employed to study carbon nanotube (CNT) FETs, SiNWFETs, and graphene nanoribbon (GNR) FETs.[16–19] The small basis suggests a limited accuracy of the energy dispersion relation and band gap, compared to the results obtained using the plane-wave Density Functional Theory (DFT) or the GW approximation, methods that use a large number of plane-waves as the basis.[20,21] Also, since empirical tight-binding requires "tuning" the hopping parameters and employs the empirically adjusted Hamiltonian matrix elements, no explicit wavefunctions are available. On the contrary, plane-wave methods can provide the full atomistic wavefunctions. Another approach, strictly related to empirical tight-binding, is based on self-consistent linear combinations of atomic orbitals (LCAO),[22] also referred to as the "density-functional tight-binding" (DF-TB) approach, in which explicit basis-functions are used. This method is usually applied to study molecular electronic devices[23] and, occasionally, small transistors consisting of ~1000 atoms.[24]

The use of pseudopotentials and a plane-wave basis presents an attractive way to calculate band structures, to obtain explicit wavefunctions, and predict current-voltage characteristics accurately for ultra-scaled devices. However, since plane-wave DFT calculations use a much larger number of plane-waves, when compared to the empirical pseudopotential method,[25] a quantum transport formalism based on local empirical pseudopotentials would be more feasible at the moment. The empirical pseudopotential method is capable of providing accurate band structures and band gaps and to simulate efficiently devices at the nanometer scale, consisting

[a]Electronic mail: jingtian.fang@utdallas.edu.
[b]Present address: Samsung Semiconductor, Inc., San Jose, California 95134, USA

of thousands of atoms. Another advantage of the empirical pseudopotential method over the plane-wave DFT consists in the possibility of "calibrating" empirical pseudopotential parameters in order to fit experimental results. Accurate values of the band gap and effective masses, for example, are of paramount importance in transport studies. Of course, this comes with some loss of predictive power when considering structures with a morphology significantly different from what is used as the "calibration point."

In very recent years, Esseni *et al.*,[26] Hueting *et al.*,[3] and Wang *et al.*[11,27] proposed methods based on the linear combination of bulk bands (LCBB). In Ref. 11, a quasi-Fermi level model and a top-of-barrier splitting model were both applied to simulate quantum transport in 10 nm and 22 nm double-gate ultra-thin-body MOSFETs. For the LCBB-quasi-Fermi level model, local thermal equilibrium is assumed. In small systems in off-equilibrium conditions, however, since each state is coherent along the whole device, the use of local states and of the local-thermal equilibrium assumption becomes invalid. Thus, the use of the quasi-Fermi level model results in a significant overestimation of the subthreshold charge density inside the channel, as well as of the current. The improved top-of-barrier model extracts scattering-state information from the stationary solution of the system. It then calculates the charge density and current. Nevertheless, the top-of-barrier model uses periodic boundary conditions and yields results agreeing well with those of the empirical tight-binding-NEGF approach using scattering state boundary conditions.[27]

In this paper, we present a quantum transport formalism based on local empirical pseudopotentials with open boundary conditions using an envelope-function approximation. Figure 1 illustrates schematically the open-boundary-condition picture on which this method rests. The outline of the formalism was presented by some of us in Ref. 28, and the formalism has been verified previously by studying SiNWs[5,29] and armchair-edge GNRs (aGNRs)[30] $n^+p^+n^+$-doped nanostructures, but without gate control and only in a one-dimensional (1D) model. Here, we extend the method to three-dimensional (3D) simulations and account for the presence of a gate with an applied bias needed to control the electrostatics of the channel. Recently, Garcia-Lekue and coworkers[12] have independently formulated the problem in a similar way.

The paper is organized as follows. The calculation of the band structure for nanostructures using the empirical pseudopotential method is briefly introduced in Sec. II A. In Sec. II B, we derive the quantum transport equations using the supercell method and the envelope-wavefunction approximation. The numerical implementation, such as the calculation of the complex band structure of the contacts and the determination of injected waves and reflected waves, is discussed in Sec. II C. Finally, in Sec. III, we discuss the example of a 3D simulation of one-dimensional electron transport in a SiNWFET with a body-size of 0.39 nm, a gate length of 6.52 nm, and an effective oxide thickness of 0.43 nm. Details about the derivations of the transport equation and of the open boundary conditions (self energies) are presented in Appendixes A and B, respectively.

II. THEORY

A. Empirical pseudopotential method for nanostructures

The empirical pseudopotential method is a plane-wave method, which relies on the periodicity of the structure to be studied. Therefore, in order to deal with nanostructures, instead of bulk solids, a cell containing many atoms is considered instead of the primitive lattice cell. By introducing vacuum around the nanostructures, a (periodic) supercell is obtained. For 1D nanostructures, we consider electrons confined in the (x-y) plane and traveling along z, so that the electron wavevector $\mathbf{k}$ reduces to a wavenumber k_z. The electron wavefunction can be written in the Bloch form $\psi(\mathbf{r}) = e^{ik_z z}\sum_{\mathbf{G}} u_{\mathbf{G}}^{k_z} e^{i\mathbf{G}\cdot\mathbf{r}}$. Using empirical pseudopotentials, the Schrödinger equation giving the energy dispersion E_{k_z} and wavefunctions is written as

$$\sum_{\mathbf{G}'}\left(\frac{\hbar^2}{2m}|\mathbf{k}+\mathbf{G}|^2\delta_{\mathbf{G}',\mathbf{G}} + V^{(1\mathrm{D})}_{\mathbf{G}',\mathbf{G}}\right)u^{k_z}_{\mathbf{G}'} = E_{k_z}u^{k_z}_{\mathbf{G}}, \qquad (1)$$

where $\mathbf{k} = (0, 0, k_z)$ and $\mathbf{G}$ denotes the translation vectors in the reciprocal space of the supercell. The number of $\mathbf{G}$-vectors $N_{\mathbf{G}}$ depends on the cut-off energy E_{cutoff} employed. The lattice potential has the form $V^{(1\mathrm{D})}_{\mathbf{G},\mathbf{G}'} = \frac{1}{\Omega}\sum_\alpha e^{-i(\mathbf{G}-\mathbf{G}')\cdot\tau_\alpha}\Omega_\alpha V^\alpha_q$, where Ω is the volume of the supercell, Ω_α is the volume of ion α in the supercell, and V^α_q is the pseudopotentials of ion α depending on $q = |\mathbf{G}-\mathbf{G}'|$. By solving Eq. (1) as an

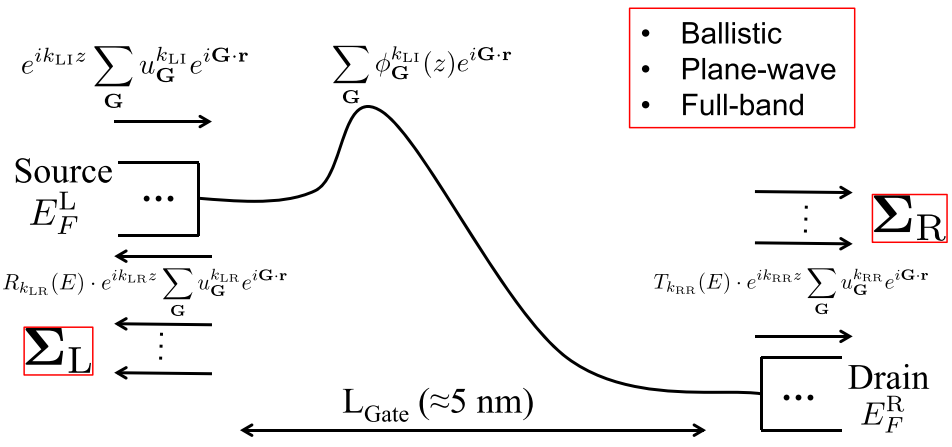

FIG. 1. Schematic plane-wave full-band quantum transport model. A wave injected at a single energy from the left contact, the multiple reflection waves, and transmitted waves are illustrated and the (asymptotic) expressions for the wavefunctions in the left and right contacts, assumed to be zero-field waveguides are shown.

eigenvalue problem, we obtain the eigenenergy E_{k_z} and the wavefunction $u_{\mathbf{G}}^{k_z}$ of each state $\mathbf{k}$. Thanks to the periodicity of the system along z, we need only to calculate the dispersion $E_{k_z}(\mathbf{k})$ in the first Brillouin zone (BZ) of the supercell.

B. Full-band plane-wave quantum transport formalism

1. Envelope-wavefunction approximation

While the supercell method is suitable to study confined systems, the envelope-wavefunction approximation[31,32] offers the possibility of applying open-boundary conditions to study electron transport within a full-band formalism. Within the approximation, the external potential is assumed not to vary appreciably over the size of a unit cell, precisely $\mathrm{d}V \ll V_{\mathrm{pseudo}} \sim 1$ Ry. Similar to the Bloch theorem, which expresses the Bloch wavefunction as a product of a plane wave $e^{i\mathbf{k}\cdot\mathbf{r}}$ with the crystal moment $\mathbf{k}$ and a modulating periodic function $u_{\mathbf{k}}(\mathbf{r})$, now the full wavefunction is expanded as

$$\psi(\mathbf{r}) = \sum_{\mathbf{G}} \phi_{\mathbf{G}}(\mathbf{r}) e^{\mathrm{i}\mathbf{G}\cdot\mathbf{r}}. \tag{2}$$

Arbitrary boundary conditions at the contacts can be applied to the envelope function components $\phi_{\mathbf{G}}(\mathbf{r})$. By coupling the envelope-wavefunction approximation with the supercell method, we can analyze structures which are homogeneous along the transport direction(s), but not necessarily homogeneous along the confinement direction(s).

2. Schrödinger equation for one-dimensional electron transport

We now extend the formulation to the case, relevant to devices, in which we introduce an external potential, $V^{(\mathrm{ext})}(\mathbf{r})$, resulting from the bias applied at the contacts. The Schrödinger equation describing electronic states in the presence of both the lattice potential energy $V^{(\mathrm{lat})}(\mathbf{r})$ and the external (Hartree) potential energy $V^{(\mathrm{ext})}(\mathbf{r})$ can be written as

$$\left[-\frac{\hbar^2}{2m}\nabla^2 + V^{(\mathrm{lat})}(\mathbf{r}) + V^{(\mathrm{ext})}(\mathbf{r})\right]\psi(\mathbf{r}) = E\psi(\mathbf{r}), \tag{3}$$

where E is the energy of the electron, $\psi(\mathbf{r})$ is the electronic wavefunction, and the Laplacian operator $\nabla^2 = \mathrm{d}^2/\mathrm{d}x^2 + \mathrm{d}^2/\mathrm{d}y^2 + \mathrm{d}^2/\mathrm{d}z^2$.

Inserting Eq. (2) into Eq. (3), we can expand the Schrödinger equation in a full-band plane-wave form

$$\sum_{\mathbf{G}} e^{i\mathbf{G}\cdot\mathbf{r}}\left\{\frac{\hbar^2}{2m}(-i\nabla + \mathbf{G})^2 + V^{(\mathrm{lat})}(\mathbf{r}) + V^{(\mathrm{ext})}(\mathbf{r})\right\}\phi_{\mathbf{G}}(\mathbf{r}) = E\sum_{\mathbf{G}} \phi_{\mathbf{G}}(\mathbf{r}) e^{i\mathbf{G}\cdot\mathbf{r}}. \tag{4}$$

Following the derivation shown in Appendix A, Eq. (4) can be written in the form

$$\sum_{\mathbf{G}'}\left\{\left[\frac{\hbar^2}{2m}(-i\nabla + \mathbf{G})^2 + V^{(\mathrm{ext})}(\mathbf{r})\right]\delta_{\mathbf{G},\mathbf{G}'} + V^{(\mathrm{1D})}_{\mathbf{G},\mathbf{G}'}\right\}\phi_{\mathbf{G}'}(\mathbf{r}) = E\phi_{\mathbf{G}}(\mathbf{r}). \tag{5}$$

For electron transport in 1D nanostructures, since $k_x = -i\mathrm{d}/\mathrm{d}x = 0$, $k_y = -i\mathrm{d}/\mathrm{d}y = 0$, Eq. (5) becomes

$$\sum_{\mathbf{G}'}\left\{\left[-\frac{\hbar^2}{2m}\frac{\mathrm{d}^2}{\mathrm{d}z^2} - \frac{\mathrm{i}\hbar^2}{m}G_z\frac{\mathrm{d}}{\mathrm{d}z}\right]\delta_{\mathbf{G},\mathbf{G}'} + W^{(\mathrm{1D})}_{\mathbf{G},\mathbf{G}'}(z)\right\}\phi_{\mathbf{G}}(z) = E^{(n)}_{k_z}\phi_{\mathbf{G}}(z), \tag{6}$$

where $E^{(n)}_{k_z}$ is the electron energy depending on k_z and band index n, $\phi_{\mathbf{G}}(z)$ is the envelope wavefunction at the energy state $E^{(n)}_{k_z}$ depending on z and $\mathbf{G}$-vectors, and the term $W^{(\mathrm{1D})}_{\mathbf{G},\mathbf{G}'}(z)$ is expressed as

$$W^{(\mathrm{1D})}_{\mathbf{G},\mathbf{G}'}(z) = V^{(\mathrm{1D})}_{\mathbf{G},\mathbf{G}'} + V^{(\mathrm{ext})}_{\mathbf{G}_{||}-\mathbf{G}'_{||}}(z) + \frac{\hbar^2|\mathbf{G}|^2}{2m}\delta_{\mathbf{G},\mathbf{G}'}. \tag{7}$$

The Hartree potential, $V^{(\mathrm{ext})}_{\mathbf{G}_{||}-\mathbf{G}'_{||}}(z)$, represents the in-plane Fourier transform of the external potential energy, $V^{(\mathrm{ext})}(\mathbf{r})$, on the cross-section at z. This is given by the expression

$$V^{(\mathrm{ext})}_{\mathbf{G}_{||}-\mathbf{G}'_{||}}(z) = \frac{1}{A}\int_A V^{(\mathrm{ext})}(\mathbf{r}) e^{-\mathrm{i}(\mathbf{G}_{||}-\mathbf{G}'_{||})\cdot\mathbf{r}_{||}}\mathrm{d}\mathbf{r}_{||}\,\delta_{G_z,G'_z}, \tag{8}$$

where $\mathbf{r}_{||}$ represents the position on the cross-section at z and A is the area of the cross-section.

Discretizing Eq. (6) in the interval $[0, L]$ employing a uniform mesh of N points and a "step size" $\Delta = L/(N-1)$, we can rewrite Eq. (6) as

$$\begin{aligned}&-\frac{\hbar^2}{2m\Delta^2}\left[\phi_{\mathbf{G}}(z_{l+1}) + \phi_{\mathbf{G}}(z_{l-1})\right]\\ &- i\frac{\hbar^2}{2m\Delta}G_z\left[\phi_{\mathbf{G}}(z_{l+1}) - \phi_{\mathbf{G}}(z_{l-1})\right]\\ &+ \frac{\hbar^2}{m\Delta^2}\phi_{\mathbf{G}}(z_l) + \sum_{\mathbf{G}'} W^{(\mathrm{1D})}_{\mathbf{G},\mathbf{G}'}(z_l)\phi_{\mathbf{G}'}(z_l) = E^{(n)}_{k_z}\phi_{\mathbf{G}}(z_l)\end{aligned} \tag{9}$$

at each point $z_l = (l-1)\Delta$ for $l = 1,2,\ldots,N$ for each $\mathbf{G}$.

Applying closed boundary conditions (i.e., $\phi_{\mathbf{G}}(z) = 0$ at $z_1 = 0$ and $z_N = L$) and recasting the equations in matrix form, we reach the eigenvalue problem

$$\begin{bmatrix} \cdot & \cdot & \cdot & \cdot & \cdot & \cdot & \cdot \\ \cdot & \mathbf{T}^- & \mathbf{D}^{l-1} & \mathbf{T}^+ & 0 & 0 & \cdot \\ \cdot & 0 & \mathbf{T}^- & \mathbf{D}^{l} & \mathbf{T}^+ & 0 & \cdot \\ \cdot & 0 & 0 & \mathbf{T}^- & \mathbf{D}^{l+1} & \mathbf{T}^+ & \cdot \\ \cdot & \cdot & \cdot & \cdot & \cdot & \cdot & \cdot \end{bmatrix}\begin{bmatrix} \cdot \\ \boldsymbol{\phi}(z_{l-1}) \\ \boldsymbol{\phi}(z_l) \\ \boldsymbol{\phi}(z_{l+1}) \\ \cdot \end{bmatrix} = E^{(n)}_{k_z}\begin{bmatrix} \cdot \\ \boldsymbol{\phi}(z_{l-1}) \\ \boldsymbol{\phi}(z_l) \\ \boldsymbol{\phi}(z_{l+1}) \\ \cdot \end{bmatrix}. \tag{10}$$

The matrix on the left-hand-side, which we shall refer to as the Hamiltonian $\mathbf{H}$, is of block-tridiagonal form and represents the Hamiltonian of the closed system. The envelope wavefunction $\boldsymbol{\phi}(z_l) = [\phi_{\mathbf{G}_1}(z_l)\, \phi_{\mathbf{G}_2}(z_l)\, \cdot\, \phi_{\mathbf{G}_{N_\mathbf{G}}}(z_l)]^\mathbf{T}$ is a column vector with $N_\mathbf{G}$ components. In the Hamiltonian $\mathbf{H}$, the discretized differential operator $\mathbf{D}^l$ at z_l is expressed as

$$\mathbf{D}^l = \begin{bmatrix} D^l_{\mathbf{G}_l} & W^{(1D)}_{\mathbf{G}_1,\mathbf{G}_2}(z_l) & W^{(1D)}_{\mathbf{G}_1,\mathbf{G}_3}(z_l) & \cdot \\ W^{(1D)}_{\mathbf{G}_2,\mathbf{G}_1}(z_l) & D^l_{\mathbf{G}_2} & W^{(1D)}_{\mathbf{G}_2,\mathbf{G}_3}(z_l) & \cdot \\ W^{(1D)}_{\mathbf{G}_3,\mathbf{G}_1}(z_l) & W^{(1D)}_{\mathbf{G}_3,\mathbf{G}_2}(z_l) & D^l_{\mathbf{G}_3} & \cdot \\ \cdot & \cdot & \cdot & \cdot \end{bmatrix}, \quad (11)$$

with $D^l_\mathbf{G} = \frac{\hbar^2}{m\Delta^2} + W^{(1D)}_{\mathbf{G},\mathbf{G}'}(z_l)$ and

$$\mathbf{T}^+ = \begin{bmatrix} T_{\mathbf{G}_1} & 0 & 0 & \cdot \\ 0 & T_{\mathbf{G}_2} & 0 & \cdot \\ 0 & 0 & T_{\mathbf{G}_3} & \cdot \\ \cdot & \cdot & \cdot & \cdot \end{bmatrix}, \quad (12)$$

with $T_\mathbf{G} = -(\frac{\hbar^2}{2m\Delta^2} + i\frac{\hbar^2 G_z}{2m\Delta})$. Note that $\mathbf{T}^- = (\mathbf{T}^+)^\dagger$ in Eq. (10). Thus, the rank of the Hamiltonian $\mathbf{H}$ is $N_\mathbf{G} \times N$.

3. Open boundary conditions

Since we are interested in the study of electron transport in an open system, we must allow for electron injection and reflection in the contact (seen as ideal reservoirs) of the transistors. Therefore, open boundary conditions, instead of closed boundary conditions, should be imposed at the boundary points z_1 and z_N in order to solve Eq. (6). Following the Quantum Transmitting Boundary Method (QTBM),[33] we derive the full-band open-boundary conditions in Appendix B.

The self-energy matrices giving information about how the structure of the reservoirs affects the wavefunctions inside the device are written as

$$[\boldsymbol{\Sigma}]_\mathrm{S} = \mathbf{T}^-[u]_\mathrm{SR}[\alpha]_\mathrm{SR}[u]^{-1}_\mathrm{SR} \quad (13)$$

for the source contact, and

$$[\Sigma]_\mathrm{D} = \mathbf{T}^+[u]_\mathrm{DR}[\alpha]_\mathrm{DR}[u]^{-1}_\mathrm{DR} \quad (14)$$

for the drain contact. In Eq. (13), the matrix $[u]_\mathrm{SR}$ is a $N_\mathbf{G} \times N_\mathbf{G}$ matrix composed of the elements $u^{k_\mathrm{SR}}_\mathbf{G}$ in Eq. (B13), where $\mathbf{G}$ is the row index indicating the $\mathbf{G}$-vector and k_SR is column index indicating the reflected wavevector in the source. This matrix represents the $N_\mathbf{G}$ Bloch components of the $N_\mathbf{G}$ reflected waves (or $N_\mathbf{G}$ transmitted waves) in the source contact at an energy $E^{(n)}_{k_z} = E(k_\mathrm{SR})$ when electrons are injected from the source (or from the drain). For the reflected propagating waves, the wavevector k_SR has a real value while for the reflected evanescent waves, k_SR is complex. In Eq. (14), the matrix $[u]_\mathrm{DR}$ is the analog of $[u]_\mathrm{SR}$ for the drain contact, which represents the $N_\mathbf{G}$ Bloch components of the $N_\mathbf{G}$ transmitted waves (or $N_\mathbf{G}$ reflected waves) in the drain contact at the energy $E^{(n)}_{k_z} = E(k_\mathrm{DR})$ when electrons are injected from the source (or from the drain). For the transmitted propagating waves, k_DR is real while for the transmitted evanescent waves k_DR is complex. The matrix $[u]^{-1}_\mathrm{SR}$ is the inverse of $[u]_\mathrm{SR}$ and $[u]^{-1}_\mathrm{DR}$ is the inverse of $[u]_\mathrm{DR}$. The matrix $[\alpha]_\mathrm{SR}$ and $[\alpha]_\mathrm{DR}$ are $N_\mathbf{G} \times N_\mathbf{G}$ diagonal matrices with the elements $e^{-ik_\mathrm{SR}\Delta}$ and $e^{-ik_\mathrm{DR}\Delta}$ on their diagonals, respectively. The terms $[\boldsymbol{\Sigma}]_\mathrm{S}$ and $[\boldsymbol{\Sigma}]_\mathrm{D}$ are the $N_\mathbf{G} \times N_\mathbf{G}$ matrices resulting from the matrix multiplication.

The inhomogeneous terms representing electron injections are

$$[\mathbf{r}.\mathbf{h}.\mathbf{s}.]^\mathrm{inj}_\mathrm{S} = ([\boldsymbol{\Sigma}]_\mathrm{S} - \mathbf{T}^-[e^{-ik_\mathrm{SI}\Delta}])[u^{k_\mathrm{SI}}_\mathbf{G}] \quad (15)$$

for the injection from the source reservoir and

$$[\mathbf{r}.\mathbf{h}.\mathbf{s}.]^\mathrm{inj}_\mathrm{D} = ([\boldsymbol{\Sigma}]_\mathrm{D} - \mathbf{T}^+[e^{ik_\mathrm{DI}\Delta}])[u^{k_\mathrm{DI}}_\mathbf{G}] \quad (16)$$

for the injection from the drain reservoir. The matrix $[u^{k_\mathrm{SI}}_\mathbf{G}]$ is a matrix of size $N_\mathbf{G} \times N_{k_\mathrm{SI}}$ representing the $N_\mathbf{G}$ Bloch components of the N_{k_SI} waves injected from the source contact at the energy $E^{(n)}_{k_z} = E(k_\mathrm{SI})$. The injected waves are propagating waves with real wavevector k_{SI}. The matrix $[u^{k_\mathrm{DI}}_\mathbf{G}]$ is a matrix of size $N_\mathbf{G} \times N_{k_\mathrm{DI}}$ representing the $N_\mathbf{G}$ Bloch components of possibly N_{k_DI} waves injected from the drain contact at the energy $E^{(n)}_{k_z} = E(k_\mathrm{DI})$. The wavevectors k_{DI} are real. Thus, $[\mathbf{r}.\mathbf{h}.\mathbf{s}.]^\mathrm{inj}_\mathrm{S}$ and $[\mathbf{r}.\mathbf{h}.\mathbf{s}.]^\mathrm{inj}_\mathrm{D}$ are matrices of rank $N_\mathbf{G} \times N_{k_\mathrm{SI}}$ and $N_\mathbf{G} \times N_{k_\mathrm{DI}}$, respectively.

The term $[\boldsymbol{\Sigma}]_\mathrm{S}$ is added to $\mathbf{D}^1$ and $[\boldsymbol{\Sigma}]_\mathrm{D}$ is added to the $\mathbf{D}^N$ in Eq. (11), and Eq. (6) is transformed into a linear system

$$(\mathbf{H} - E^{(n)}_{k_z}\mathbf{I} + [\boldsymbol{\Sigma}]_\mathrm{S} + [\boldsymbol{\Sigma}]_\mathrm{D})\boldsymbol{\phi} = [\mathbf{r}.\mathbf{h}.\mathbf{s}.]^\mathrm{inj}_\mathrm{S} + [\mathbf{r}.\mathbf{h}.\mathbf{s}.]^\mathrm{inj}_\mathrm{D}, \quad (17)$$

when we apply the open boundary conditions. In Eq. (17), $\mathbf{I}$ is the identity matrix, and $\boldsymbol{\phi} = [\boldsymbol{\phi}(z_1)\, \boldsymbol{\phi}(z_2)\, \cdot\, \boldsymbol{\phi}(z_N)]^\mathbf{T}$.

4. Charge and potential distribution

By solving Eq. (17) for an injection state $\mathbf{k} = (0, 0, k_z)$ at the band n with an energy $E^{(n)}_{k_z}$, the full wavefunction $\psi^{(n)}_{k_z}(\mathbf{r})$ is calculated from $\phi^{k_z}_\mathbf{G}(z)$ using Eq. (2) and the electron density is computed as

$$n(\mathbf{r}) = \frac{1}{\pi}\sum_n \sum_{\nu=\mathrm{S,D}} \int_{1\mathrm{stBZ}} |\psi^{(n)}_{k_z}(\mathbf{r})|^2 f\left(E^{(n)}_{k_z}, E^\nu_F\right) \mathrm{d}k_z. \quad (18)$$

In this expression, the sum is performed only over the occupied states in the conduction band, since the charge of the occupied valence states is already implicitly accounted for by the empirical nature of the pseudopotentials we employ. We account for electron injection from the source ($\nu = \mathrm{S}$) and drain ($\nu = \mathrm{D}$) contacts. The occupation of the injected state at energy $E^{(n)}_{k_z}$ is determined by its thermal-equilibrium Fermi-Dirac occupation, $f(E^{(n)}_{k_z}, E^\nu_F)$, via the Fermi level E^ν_F in the contacts.

In order to treat transport self-consistently, we start from a initial guess of $V^{(\mathrm{ext})}(\mathbf{r})$ and solve Eq. (17). The density $n(\mathbf{r})$ is then obtained from Eq. (18). To obtain a new $V^{(\mathrm{ext})}(\mathbf{r})$

for the next iteration, we use Newton's method to solve the Poisson equation

$$\mathbf{J}\cdot\delta V^{(\mathrm{ext})}(\mathbf{r})=\delta\rho(\mathbf{r}) \tag{19}$$

and obtain the change of external potential energy as $\delta V^{(\mathrm{ext})}(\mathbf{r})$. In Eq. (19), $\mathbf{J}$ is the Jacobian matrix and $\rho(\mathbf{r})=N_{\mathrm{D}}(\mathbf{r})-n(\mathbf{r})-N_{\mathrm{A}}(\mathbf{r})+p(\mathbf{r})$, where $N_{\mathrm{D}}(\mathbf{r})$ is the donor density, $N_{\mathrm{A}}(\mathbf{r})$ is the acceptor density in the device, $p(\mathbf{r})$ is the hole density calculated in a way similar to $n(\mathbf{r})$. We solve Eq. (17) with the new $V^{(\mathrm{ext})}(\mathbf{r})$ and iterate the procedure till convergence with a criterion on the error of $\delta V^{(\mathrm{ext})}(\mathbf{r})$ is reached. The numerical implementation yielding convergence, such as the specific form of the Jacobian matrix $\mathbf{J}$, will be discussed in detail in Sec. II C 3.

5. Device characteristics

Once a self-consistent solution is found, the device current can be calculated from the known envelope wavefunctions. The current flowing from the source contact to the drain contact is given by the expression

$$I_{\mathrm{S}\to\mathrm{D}}(z)=\frac{1}{\pi}\sum_{n}\int_{1\mathrm{stBZ}}j_{k_z}^{(n)}(z)f\left(E_{k_z}^{(n)},E_F^{\mathrm{S}}\right)\times\left[1-f\left(E_{k_z}^{(n)},E_F^{\mathrm{D}}\right)\right]\mathrm{d}k_z\,. \tag{20}$$

A similar expression holds for the current flowing from the drain to the source, $I_{\mathrm{D}\to\mathrm{S}}(z)$. The total device current is obtained by adding the two currents, $I(z)=I_{\mathrm{S}\to\mathrm{D}}(z)-I_{\mathrm{D}\to\mathrm{S}}(z)$. In Eq. (20), $j_{k_z}^{(n)}(z)$ is the current density

$$j_{k_z}^{(n)}(z)=\frac{\mathrm{i}\hbar}{2m}\sum_{\mathbf{G}}\left(\phi_{\mathbf{G}}^{k_z}(z)\right)^{\star}\left(\frac{\mathrm{d}\phi_{\mathbf{G}}^{k_z}(z)}{\mathrm{d}z}+\mathrm{i}G_z\phi_{\mathbf{G}}^{k_z}(z)\right). \tag{21}$$

The transmission and reflection coefficients for the injected waves also provide information about the tunneling probability in the device. For the source contact injection, the transmission coefficient is given by the expression

$$T_{\mathrm{S}\to\mathrm{D}}(E_{k_z}^{(n)})=\sum_{N_{k_{\mathrm{SI}}}}[v_{k_{\mathrm{DR}}}]|[u]_{\mathrm{DR}}^{-1}[\phi_{\mathbf{G}}^{k_{\mathrm{SI}}}(L)]|^2/v_{k_{\mathrm{SI}}}\,, \tag{22}$$

where $v_{k_{\mathrm{DR}}}$ is the group velocity of the transmitted propagating wave, $\phi_{\mathbf{G}}^{k_{\mathrm{SI}}}(L)$ are the envelope functions at the drain contact, and $v_{k_{\mathrm{SI}}}$ is the group velocity of the injected wave. The reflection coefficient is given by

$$R_{\mathrm{S}}(E_{k_z}^{(n)})=\sum_{N_{k_{\mathrm{SI}}}}[v_{k_{\mathrm{SR}}}]|[u]_{\mathrm{SR}}^{-1}([\phi_{\mathbf{G}}^{k_{\mathrm{SI}}}(0)]-[u_{\mathbf{G}}^{k_{\mathrm{SI}}}])|^2/v_{k_{\mathrm{SI}}}\,, \tag{23}$$

where $v_{k_{\mathrm{SR}}}$ is the group velocity of the reflected propagating wave, and $\phi_{\mathbf{G}}^{k_{\mathrm{SI}}}(0)$ are the envelope functions at the source contact.

C. Numerical implementation

The flow chart for solving Eq. (17) self-consistently is shown in Fig. 2. Assuming that a starting external potential $V^{(\mathrm{ext})}(\mathbf{r})$ is somehow given (from a semiclassical solution, a solution at a previous bias, etc.), we can build the Hartree potential at first using Eq. (8). Then, the band structure of the source contact is obtained from Eq. (1), adding to it $V_{\mathbf{G}_{\parallel}-\mathbf{G}'_{\parallel}}^{(\mathrm{ext})}(0)$, and the band structure of the drain contact is similarly solved using Eq. (1) including $V_{\mathbf{G}_{\parallel}-\mathbf{G}'_{\parallel}}^{(\mathrm{ext})}(L)$. This yields the energy $E_{k_z}^{(n)}$ of electrons injected from the reservoirs. For the energy state $E_{k_z}^{(n)}$, the self-energies and inhomogeneous injection terms are constructed from the Bloch eigenvectors $u_{\mathbf{G}}^{k_{\mathrm{Sp}}}$ and $u_{\mathbf{G}}^{k_{\mathrm{Dp}}}$ (p = I for injected waves and p = R for reflected waves) of the source and drain contacts using Eqs. (13)–(16). In Sec. II C 1, we shall show how these eigenvectors can be calculated from the complex band structure of both contacts. We also discuss how to select propagating waves (including the injected waves and part of the reflected waves) with a real $k_{\mathrm{S(D)p}}$ and evanescent waves (part of the reflected waves) with a complex $k_{\mathrm{S(D)p}}$ from the eigenvalues we obtain in Sec. II C 2. In Sec. II C 3, we discuss how to achieve the convergence in the self-consistent calculation.

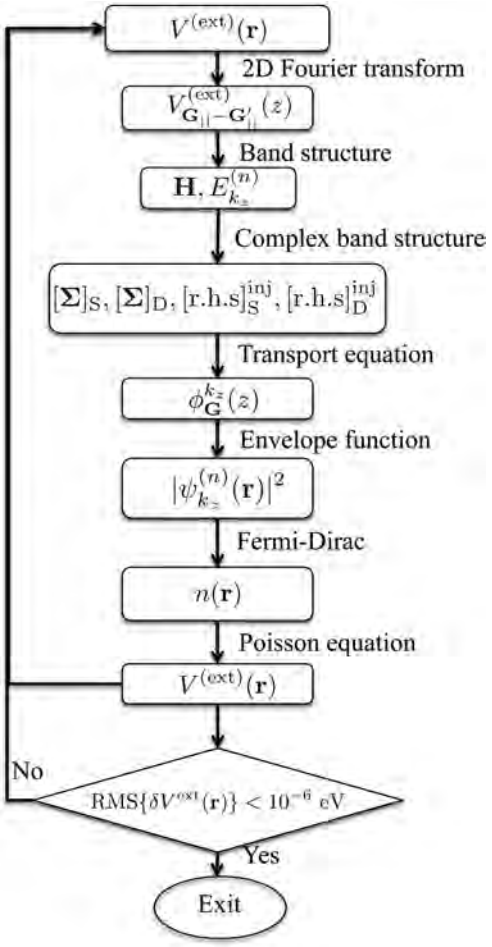

FIG. 2. Flow chart for solving the one-dimensional full-band plane-wave quantum transport Schrödinger equation and the three-dimensional Poisson's equation self-consistently.

1. Discretized band structure calculation, real and complex

When formulating the open-boundary-condition Schrödinger problem using a single-band model (e.g., the effective-mass

approximation), only propagating waves—injected, reflected, and transmitted—need to be considered. This is not true when using a multi-band model, since the reflected and transmitted waves can be superpositions of propagating and evanescent waves, the latter ones corresponding to complex wavevectors. Therefore, the problem must be formulated so as to allow the contacts to absorb not only propagating waves but also evanescent waves. This, in turn, obviously requires the knowledge of the energy dispersion not only for real but also for complex wavevectors. In other words, we need to calculate the full complex band structure of the contacts in order to account properly for the open boundary conditions. We obtain the complex band structure following the method presented in Ref. 34.

From the discretized form of Eq. (17), we must consider the transport equation

$$\mathbf{T}^{-}\boldsymbol{\phi}(z_{l-1}) + (\mathbf{D}^{l} - E^{(n)}_{k_z}\mathbf{I})\boldsymbol{\phi}(z_l) + \mathbf{T}^{+}\boldsymbol{\phi}(z_{l+1}) = 0 \tag{24}$$

at the point z_l. Since $\boldsymbol{\phi}(z_{l+1}) = e^{ik_z\Delta}\boldsymbol{\phi}(z_l)$ and $\boldsymbol{\phi}(z_{l-1}) = e^{-ik_z\Delta}\boldsymbol{\phi}(z_l)$ hold for traveling Bloch waves, replacing $\boldsymbol{\phi}(z_{l+1})$ and $\boldsymbol{\phi}(z_{l-1})$ in Eq. (24) leads to

$$(e^{-ik_z\Delta}\mathbf{T}^{-} + \mathbf{D}^{l} + e^{ik_z\Delta}\mathbf{T}^{+})\boldsymbol{\phi}(z_l) = E^{(n)}_{k_z}\boldsymbol{\phi}(z_l)\,. \tag{25}$$

We can calculate the discretized band structure by solving this equation. Similarly, by replacing $\boldsymbol{\phi}(z_{l+1}) = e^{2ik_z\Delta}\boldsymbol{\phi}(z_{l-1})$ and $\boldsymbol{\phi}(z_l) = e^{ik_z\Delta}\boldsymbol{\phi}(z_{l-1})$ in Eq. (24), we obtain

$$\begin{bmatrix} 0 & \mathbf{I} \\ -\mathbf{T}^{-}(\mathbf{T}^{+})^{-1} & -(\mathbf{D}^{l} - E^{(n)}_{k_z}\mathbf{I})(\mathbf{T}^{+})^{-1} \end{bmatrix} \begin{bmatrix} \boldsymbol{\phi}(z_{l-1}) \\ e^{ik_z\Delta}\boldsymbol{\phi}(z_{l-1}) \end{bmatrix} = e^{ik_z\Delta}\begin{bmatrix} \boldsymbol{\phi}(z_{l-1}) \\ e^{ik_z\Delta}\boldsymbol{\phi}(z_{l-1}) \end{bmatrix}, \tag{26}$$

which is also an eigenvalue equation whose solution yields the discretized complex band structure at z_{l-1}.

For the electron injection from the source contact, solving Eq. (26) at the energy $E^{(n)}_{k_z}$ both at the source contact ($l=1$, $z_0=-\Delta$) and at the drain contact ($l=N$, $z_{N-1}=L-\Delta$), we obtain $2N_{\mathbf{G}}$ eigenvalues $\alpha_S = e^{ik_S\Delta}$, $2N_{\mathbf{G}}$ Bloch eigenvectors $\boldsymbol{\phi}(z_0)$, and the same number of eigenvalues $\alpha_D = e^{ik_D\Delta}$ and eigenvectors $\boldsymbol{\phi}(z_{N-1})$.

2. Determination of injected, reflected, transmitted, and evanescent waves

In order to construct the self-energies, Eqs. (13) and (14), we need to choose the $N_{\mathbf{G}}$ solutions (out of the $2N_{\mathbf{G}}$ solutions of α_S from Eq. (26)) corresponding to injected and reflected components (propagating or evanescent) at the source contact, and similarly at the drain contact.

We can first determine whether the waves are propagating or evanescent from the magnitude of α_S, $|\alpha_S|$, and the magnitude of α_D, $|\alpha_D|$. For propagating waves with a real k_S and k_D, $|\alpha_S|$ and $|\alpha_D|$ are unity. On the contrary, evanescent waves in the contacts are associated to a complex k_S and k_D, with $|\alpha_S| > 1$ for reflected evanescent waves in source contact and $|\alpha_D| < 1$ for the transmitted evanescent waves in drain contact.

Among the propagating waves at the source contact, we determine if they are injected waves or reflected waves from the group velocity v_{k_S} or equivalently the probability current-density. The probability current density is calculated from Eq. (21), but replacing $\phi^{k_z}_{\mathbf{G}}(z)$ with the eigenvectors $\boldsymbol{\phi}(\mathbf{z_0})$ or $\boldsymbol{\phi}(z_{N-1})$ obtained from Eq. (26). For the source contact, the probability current density at $z_1 = 0$ is

$$\begin{aligned} j^{(n)}_{k_z}(0) &= \frac{i\hbar}{2m}\sum_{\mathbf{G}}\left(\boldsymbol{\phi}(z_1)\right)^{\star}\left(\frac{\mathrm{d}\boldsymbol{\phi}(z_1)}{\mathrm{d}z} + iG_z\boldsymbol{\phi}(z_1)\right) \\ &= \frac{i\hbar}{2m}\sum_{\mathbf{G}}\left(\alpha_L\boldsymbol{\phi}(z_0)\right)^{\star}\left(\frac{\alpha_L^2-1}{2\Delta}\boldsymbol{\phi}(z_0) + iG_z\frac{\alpha_L^2+1}{2}\boldsymbol{\phi}(z_0)\right), \end{aligned} \tag{27}$$

since $\boldsymbol{\phi}(z_1) = e^{ik_S\Delta}\boldsymbol{\phi}(z_0) = \alpha_S\boldsymbol{\phi}(z_0)$. The wave packet $e^{ik_S\Delta}$ represents an injected wave if $j^{(n)}_{k_z}(0) > 0$ and we label it as $\alpha_{SI} = e^{ik_{SI}\Delta}$ with a group velocity $v_{k_{SI}}$ and the eigenvector is $[u^{k_{SI}}_{\mathbf{G}}] = \alpha_{SI}\boldsymbol{\phi}(z_0)$. If $j^{(n)}_{k_z}(0) < 0$, it is a reflected propagating wave. We label the determined reflected evanescent waves and reflected propagating waves as $\alpha_{SR} = e^{ik_{SR}\Delta}$ with a group velocity $v_{k_{SR}}$ and the eigenvector is $[u^{k_{SR}}_{\mathbf{G}}] = \alpha_{SR}\boldsymbol{\phi}(z_0)$. The group velocity of the evanescent waves $v_{k_{SR}}$ is 0 since they do not carry current.

The current density at $z_N = L$, $j^{(n)}_{k_z}(L)$, is calculated in the same way as Eq. (27), but replacing $\boldsymbol{\phi}(z_1)$ with $\boldsymbol{\phi}(z_N) = \alpha_D\boldsymbol{\phi}(z_{N-1})$. The wave packet $e^{ik_D\Delta}$ represents a transmitted propagating wave if $j^{(n)}_{k_z}(L) > 0$. We label these transmitted propagating waves and evanescent waves as $\alpha_{DR} = e^{ik_{DR}\Delta}$ with the group velocity $v_{k_{DR}}$. The eigenvectors $[u^{k_{DR}}_{\mathbf{G}}]$ are equal to $\alpha_{DR}\boldsymbol{\phi}(z_{N-1})$. For the transmitted evanescent waves, the group velocity $v_{k_{DR}}$ is 0 since they do not carry any current. The open boundary conditions for the drain contact injection can be constructed in the same way.

3. Self-consistent calculation

As shown in Fig. 2, the self-consistent procedure is performed by iteratively updating $V^{(\mathrm{ext})}(\mathbf{r})$ and $n(\mathbf{r})$. The iteration procedure stops when the root-mean-square of $\delta V^{(\mathrm{ext})}(\mathbf{r})$ is less than a set convergence criterion.

Specifically, having solved the transport equation, we perform a 3D Fourier transform of $\phi^{k_z}_{\mathbf{G}}(z)$ for each slice at z, thus obtaining the full wavefunction $\psi^{k_z}(\mathbf{r})$. In the spirit of the envelope-wavefunction approximation, we then consider a coarse-grained averaged electron density by averaging over a unit cell along z the squared amplitude of the full wavefunction. The induced charge density and potential are smooth enough to enable convergence of the self-consistent calculation. To solve Poisson equation, Newton's method and the semiclassical Jacobian matrix

$$\mathbf{J} = \nabla^2 - \frac{e^2}{\epsilon}\frac{\mathrm{d}\rho(\mathbf{r})}{\mathrm{d}V^{(\mathrm{ext})}(\mathbf{r})} \approx \nabla^2 - \frac{e^2}{\epsilon}\frac{n(\mathbf{r})}{k_BT} \tag{28}$$

based on random phase approximation are used. A uniform dielectric constant ϵ is assumed.

It is worth mentioning that the method for charge density calculation described above is different from what is proposed in Sec. II B 4. We should comment why performing a cell-average along z of the electron density (a choice different from the "ideal" method described in Sec. II B 4) is not only consistent with the envelope approximation but also necessary for numerical reasons. The discretization step Δ along z has to satisfy simultaneously two opposite requirements. On one hand, it should be small enough to resolve the variation of the electron density at the atomic scale and also to guarantee an accurate numerical integration of the transport equation. On the other hand, a value of Δ much smaller than the lattice constant corresponds to values of the wavevector (or wavenumber k_z) outside the first Brillouin zone. This would result in the appearance of "ghost states" associated with unphysical spurious states outside the first BZ. This is due to the finite number of reciprocal lattice vectors we employ, and the associated loss of periodicity along z. This is not a problem in the calculation of the band structure of bulk crystals, since one usually employs a "moving sphere" centered around the **k**-point of interest and with radius determined by the energy cutoff. In our case, instead, in order to obtain a manageable size of the problem, we must consider only **G**-vectors corresponding to a unit cell along the axial (transport) direction and the use of a "moving sphere" is prevented by the fact that k_z is replaced by $-i\nabla_z$. Therefore, we must abandon the idea of obtaining the charge density at an atomic resolution and employ a value of Δ of the order of the lattice constant. This avoids the problem of dealing with spurious solutions. At the same time, this choice provides a sufficiently accurate resolution of the external potential that, by our initial assumption on which the envelope approximation is based, varies slowly over a unit cell.

III. RESULTS

We apply the formalism introduced in Sec. II to study a gate-all-around (GAA) (3×3)-SiNWFET with electron transport along the [001] axial direction. The device length is 21.72 nm, the gate length, L_G, is 6.52 nm, the effective oxide thickness is 0.43 nm, and the body size characterized with the NW side length is 0.39 nm. The device is $n^+p^+n^+$ doped along z. The donor density in the source and the drain contacts is $1.0 \times 10^8\,\mathrm{m}^{-1}$, and the acceptor density in the gate contact is $1.0 \times 10^8\,\mathrm{m}^{-1}$.

A. Atomic structure of the channel material and energy band structure

The model of the [001]-oriented SiNW channel with a square cross-section and hydrogen-passivated {110} surfaces is shown in Fig. 3. Since the wire consists of three monolayers along both sides of the square, we denote it as a (3×3)-SiNW. The body size of the nanowire is defined by its side-length of 0.386 nm. The terminating hydrogen atoms are located at positions which still maintain the original tetrahedral coordination with a Si-H bond length $0.158\sqrt{3}a_0 = 0.149$ nm, where $a_0 = 0.543$ nm is the lattice constant of bulk silicon. The vacuum distance, including the spacing of the hydrogens, between the sides of the supercell is 0.768 nm, which is large enough to suppress the interaction between neighboring wires, since there is no electronic wavefunction overlap.

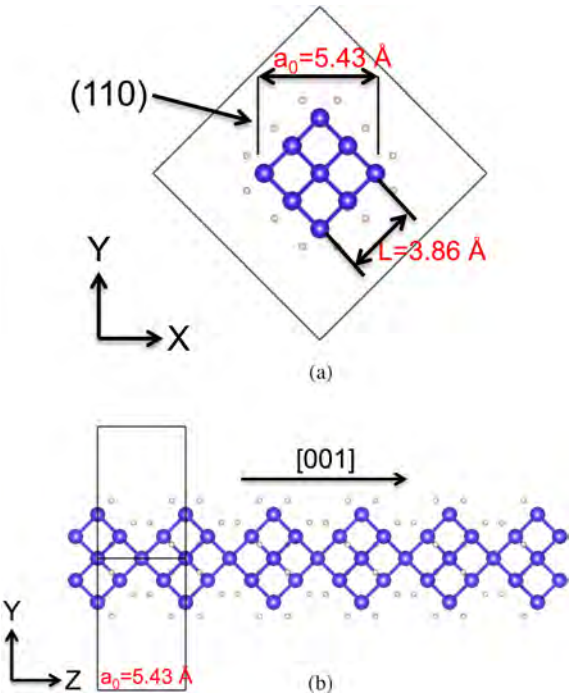

FIG. 3. Atomistic model of a (3×3) [001]-oriented SiNW with {110} surfaces. The cross-section has a square shape and the side length of the nanowire body is 0.386 nm. The distance from the sides of the nanowire to the sides of the square supercell is also 0.386 nm. The translation vector along z is the lattice constant of bulk silicon, 0.543 nm.

Ignoring the structural relaxation of the atomic configurations, which may be significant especially for the surface atoms, and by solving Eq. (1) using the local empirical pseudopotentials,[35,36] the band structure of the nanowire is calculated using a cutoff energy E_{cutoff} of 4.5 Ry, resulting in $N_{\mathbf{G}} = 783$. This is shown in Fig. 4. The electronic states in this nanowire are strongly confined and exhibit significant valley-splitting.[37] The band gap takes a value of 4.6 eV, much larger than the gap of bulk Si, because of quantum

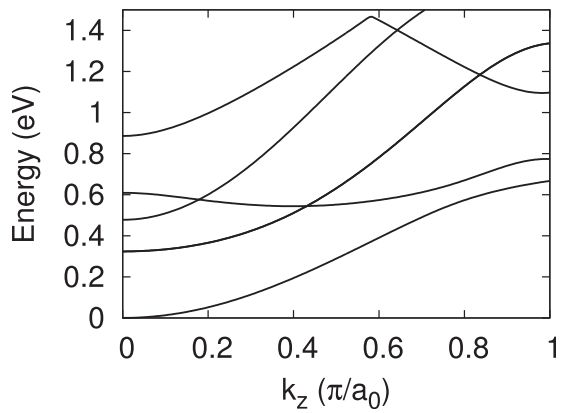

FIG. 4. Band structure of a (3×3)-SiNW only considering the lattice potential using $E_{\mathrm{cutoff}} = 4.5$ Ry. The six lowest-energy conduction bands are shown. Energy of the bottom of the conduction band is set to zero. The second conduction band is ~300 meV away from the bottom of the conduction band. For low-energy electron transport, only the lowest conduction band is occupied.

confinement. And the gap is indirect since the valence band reaches its maximum when the wavevector (wavenumber) is at the zone edge, while the conduction band minimum is located at the center of the BZ (that is, at the Γ symmetry point).

B. Transport characteristics of (3 × 3)-SiNWFET

In order to solve numerically the transport equation, the device is discretized into $N = 81$ slices along z with a mesh size $\Delta = 21.72/80 = 0.27$ nm, which is half of the lattice constant. In order to solve Poisson equation, a 2D triangular finite-element mesh is generated in each slice, and the 3D finite-element mesh with prismatic elements is obtained by extruding the 2D mesh along z. Dirichlet boundary conditions are applied at the gate contact. A uniform **k**-space mesh with the discretization step $\Delta k_z = 0.005(2\pi/a_0)$ results in 94 injection energy states from the bottom of the conduction band E_c to $E_c + 10k_BT$. A uniform dielectric constant of 3.48 is assumed to obtain the effective oxide thickness of 0.43 nm.

The iteration to obtain a self-consistent solution starts with $V^{(ext)}(\mathbf{r}) = 0$. After solving the transport equation for all the injection energies, the corresponding envelope wavefunctions are obtained. In Fig. 5, we show the squared amplitude of the envelope wavefunctions averaged over a unit cell as a function of z for a few selected injection energies at $V_{GS} = 0$ V and $V_{DS} = 0.1$ V. These wavefunctions are obtained by summing the coefficients $|\phi^{k_z}_{\mathbf{G}}(z)|^2$ over all the **G**-vectors. As expected, low-energy electrons exhibit long wavelengths and the amplitude of the associated wavefunctions decays in the potential barrier. On the contrary, the wavefunctions associated with high-energy electrons exhibit an almost constant amplitude close to unity.

The charge density and potential energy profile along the transport direction are shown in Fig. 6. Charge neutrality is preserved near the contacts, thanks to the Neumann boundary conditions imposed on the Poisson equation. This choice of boundary conditions is equivalent to the shift of the Fermi level employed by Poetz.[38] The problem of maintaining charge neutrality near the contacts in quantum ballistic simulations has been discussed at length by Frensley[39] and Fischetti.[40] To evaluate the drain-induced barrier-lowering (DIBL), in Fig. 7, we show the potential energy profile at $V_{GS} = 0$ V and different V_{DS}. The potential barrier is lowered with an amount of 0.48 mV when V_{DS} is increased from 0.01 V to 0.2 V, corresponding to a negligible DIBL of 2.5 mV/V on average, which indicates that there is an excellent electrostatic control on the gate for the GAA architecture of the device.

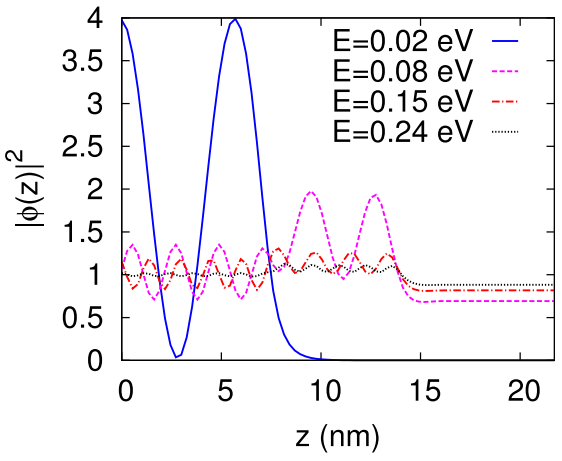

FIG. 5. Square of the envelope functions along z at several energy states for the source contact injection at $V_{GS} = 0$ V and $V_{DS} = 0.1$ V.

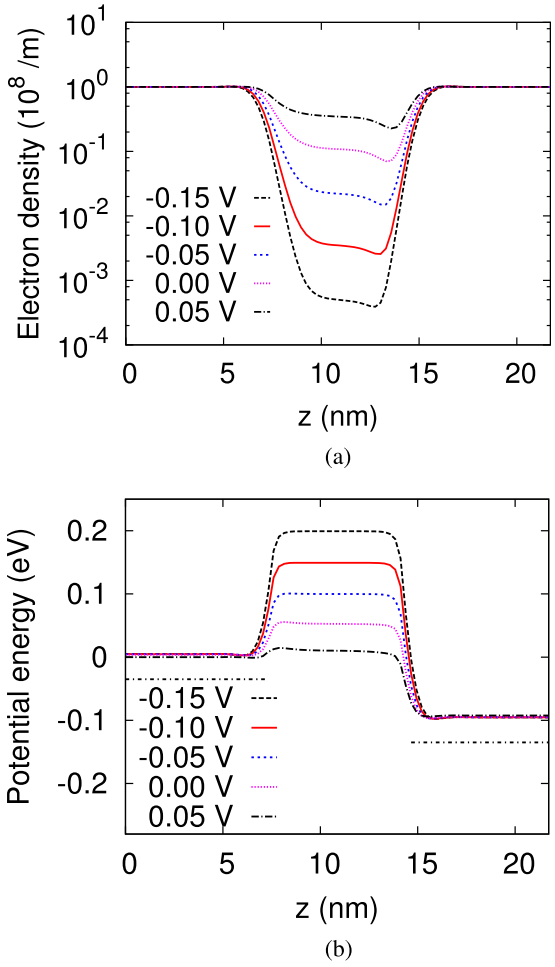

FIG. 6. (a) One-dimensional charge density distribution, obtained by averaging the three-dimensional charge density n(**r**) in each cross-section, along z at $V_{DS} = 0.1$ V and V_{GS} ranging from −0.15 V to 0.05 V. (b) One-dimensional potential energy profile along z. The short dashed line below the energy profile is the Fermi level in the source and drain contact, respectively.

The reflection and transmission coefficients are plotted in Fig. 8. In general, the transmission coefficient increases as the electron injection energy increases. However, it is interesting to note the appearance of resonances in the transmission probability. These are loosely related to the Wigner-Breit resonances[41] and are due to the interference of incoming waves with waves reflected by the sharp drop of the potential energy at the channel-drain junction. Similar effects have been observed experimentally in Fowler-Nordheim tunneling in SiO_2 films.[42] Ultimately, since this sharp drop is due to the excellent electrostatic control of the gate on the channel potential, these

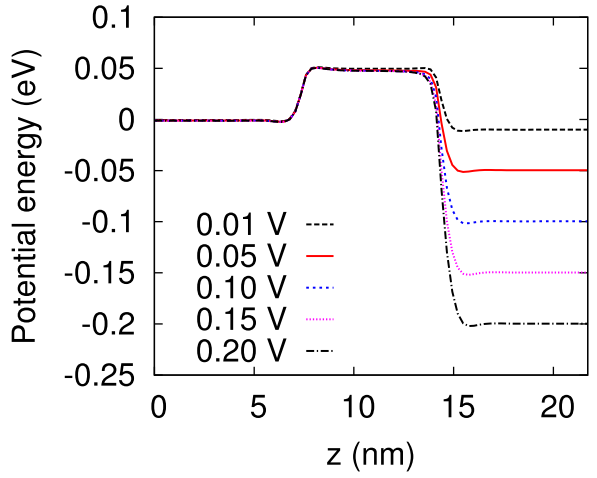

FIG. 7. One-dimensional potential energy profile along z at $V_{GS} = 0$ V and V_{DS} ranging from 0.01 V to 0.20 V.

resonances emphasize the good quality of the GAA geometry. Of course, they appear only when the electron coherence is maintained over the entire length of the channel, so it is doubtful whether these resonances lead to any observable effect.

The I_{DS}–V_{GS} and I_{DS}–V_{DS} characteristics of the device are shown in Fig. 9, indicating that the device has a subthreshold slope (SS) of 66 mV/dec. From Fig. 9(b), we see that the current increases linearly at low V_{DS} and saturates at high V_{DS}. For $V_{GS} = 0.05$ V in the subthreshold region, the saturation current is 0.28 μA. When scaling it to the circumference of the nanowire, the current density is 190 μA/μm. In the calculation, obviously, the **k**-space discretization affects the number of injection energy states. We have verified that modifying the number of injected waves by changing the k_z-spacing Δk_z from $0.005(2\pi/a)$ to $0.01(2\pi/a)$, and so using 47 instead of 94 injection energies at the source contact, the current does not change appreciably.

Regarding the numerics of the simulation, the rank of the block-tridiagonal matrix is $N_{\mathbf{G}} \times N = 783 \times 81 = 63\,423$ and the number of non-zero element in the sparse

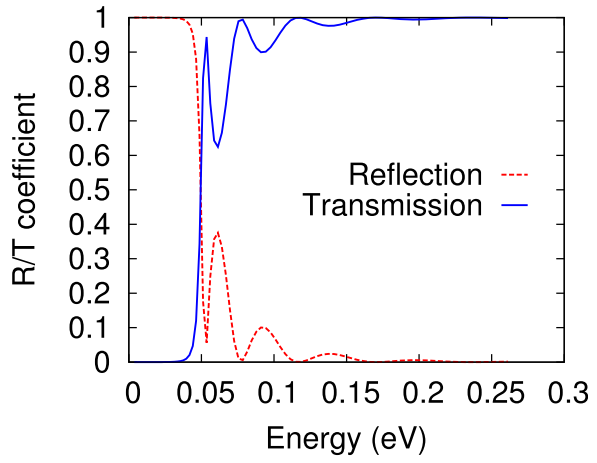

FIG. 8. Energy-dependent reflection and transmission coefficient for the source contact injection at $V_{GS} = 0$ V and $V_{DS} = 0.1$ V. At certain energies, the electron waves resonate inside the device.

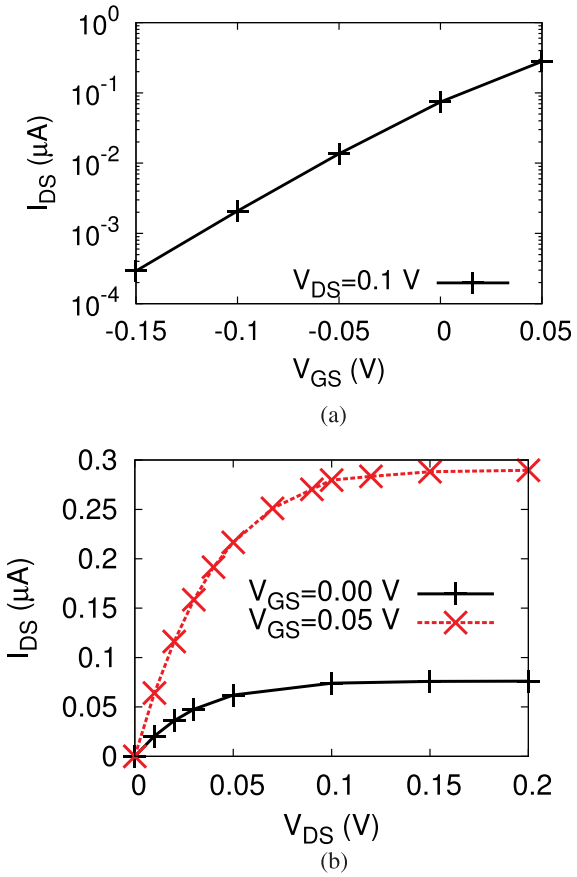

FIG. 9. (a) I_{DS}–V_{GS} characteristics of the (3×3)-SiNWFET. The device has a subthreshold slope ~66 mV/dec. (b) I_{DS}–V_{DS} characteristics of the (3×3)-SiNWFET at $V_{GS} = 0$ V and 0.05 V. The current is linearly increasing at low V_{DS} and saturates at high V_{DS}.

matrix is $N_{\mathbf{G}}^2 \times N + (N-1) \times 2N_{\mathbf{G}} = 49\,785\,489$. We performed the computation on an IBM P55 POWER 7 cluster. When 94 energies states are injected from either contact, we assign 94 cores to solve the transport equation in parallel. For each injection energy from the source or drain contact, about 300 s are required to construct the open-boundary conditions. Using a linear-system sparse matrix solver UMFPACK,[43] the large-scale linear equation is solved efficiently in about 300 s. Therefore, for a single self-consistent loop considering both source and drain contact injections, about 1200 s are required to solve the transport equations. In total, approximately ~10 hours are required to reach convergence in 28 self-consistent loops for the potential energy with a criterion $\sqrt{\sum_{N_{3D}} |\delta V^{(\mathrm{ext})}(\mathbf{r})|^2 / N_{3D}} < 10^{-6}$ eV at a single V_{DS} and V_{GS}, where N_{3D} is the number of points in **r**-space of the device. The maximum memory requirement for each core is about 6GB during the UMFPACK LU factorization.

IV. CONCLUSIONS

We have presented a full-band plane-wave quantum transport formalism based on empirical pseudopotentials. We have shown how to construct open-boundary conditions using the full complex band structure at the contacts and how to calculate the charge density and device current from

the electronic wavefunctions obtained from the transport equation. As an example, we have applied this formalism to a GAA SiNWFET with an extremely small body size and a short channel length.

ACKNOWLEDGMENTS

This work has been supported in part by Samsung Electronics Ltd. and by the Nanoelectronics Research Initiative's (NRI's) Southwest Academy of Nanoelectronics (SWAN) center affiliated with the Semiconductor Research Corporation (SRC).

APPENDIX A: DERIVATION OF THE TRANSPORT EQUATION

Multiplying Eq. (4) by $e^{-i\mathbf{G}'\cdot\mathbf{r}}$ on both sides for each $\mathbf{G}$ and integrating over $\mathbf{r}$ over a single cell with the origin at $\mathbf{r}_l$, the first term on the left-hand side (l.h.s) becomes

$$\frac{\hbar^2}{2m}\int_{\Omega_c} \mathrm{d}\mathbf{r}\, e^{i(\mathbf{G}-\mathbf{G}')\cdot\mathbf{r}}\,(-i\nabla+\mathbf{G})^2\phi_{\mathbf{G}}(\mathbf{r}), \tag{A1}$$

where Ω_c is the volume of a unit cell. Thanks to the assumption that $\phi_{\mathbf{G}}(\mathbf{r})$ is slowly varying over a unit cell along the z-direction, we can treat it as a constant over a unit cell when integrated over the fast-oscillating function $e^{i\mathbf{G}\cdot\mathbf{r}}$. Then, Eq. (A1) is simplified to

$$\frac{\hbar^2}{2m}(-i\nabla+\mathbf{G})^2\phi_{\mathbf{G}}(\mathbf{r}_l)\int_{\Omega_c}\mathrm{d}\mathbf{r}\, e^{i(\mathbf{G}-\mathbf{G}')\cdot\mathbf{r}} = \Omega_c\,\frac{\hbar^2}{2m}(-i\nabla+\mathbf{G})^2\,\phi_{\mathbf{G}}(\mathbf{r}_l)\,\delta_{\mathbf{G},\mathbf{G}'}. \tag{A2}$$

Similarly, the third term at the l.h.s of Eq. (4) can be written as

$$\int_{\Omega_c}\mathrm{d}\mathbf{r}e^{i(\mathbf{G}-\mathbf{G}\prime)\cdot\mathbf{r}}V^{(\mathrm{ext})}(\mathbf{r})\phi_{\mathbf{G}}(\mathbf{r}) = \Omega_c V^{\mathrm{ext}}(\mathbf{r}_l)\phi_{\mathbf{G}}(\mathbf{r}_l)\delta_{\mathbf{G},\mathbf{G}'}. \tag{A3}$$

Integrating $V^{(\mathrm{lat})}(\mathbf{r})$ over a unit cell yields

$$\int_{\Omega_c}\mathrm{d}\mathbf{r}e^{i(\mathbf{G}-\mathbf{G}\prime)\cdot\mathbf{r}}V^{(\mathrm{lat})}(\mathbf{r})\phi_{\mathbf{G}}(\mathbf{r}) = \Omega_c V_{\mathbf{G}'-\mathbf{G}}\phi_{\mathbf{G}}(\mathbf{r}_l). \tag{A4}$$

The integration on the right-hand side (r.h.s.) of Eq. (4) yields

$$\int_{\Omega_c}\mathrm{d}\mathbf{r}\, e^{i(\mathbf{G}-\mathbf{G}\prime)\cdot\mathbf{r}}\,\phi_{\mathbf{G}}(\mathbf{r}) = \Omega_c\,\phi_{\mathbf{G}}(\mathbf{r}_l)\delta_{\mathbf{G},\mathbf{G}'}. \tag{A5}$$

Gathering all terms, Eq. (4) takes the form of an eigenvalue problem

$$\sum_{\mathbf{G}}\left\{\left[\frac{\hbar^2}{2m}(-i\nabla+\mathbf{G})^2+V^{(\mathrm{ext})}(\mathbf{r})\right]\delta_{\mathbf{G},\mathbf{G}'}+V_{\mathbf{G}'-\mathbf{G}}\right\}\cdot\phi_{\mathbf{G}}(\mathbf{r}) = E\phi_{\mathbf{G}'}(\mathbf{r}). \tag{A6}$$

APPENDIX B: FULL-BAND OPEN BOUNDARY CONDITIONS

We consider a wire which is in contact with a source reservoir ($z<0$) denoted as S afterwards and a drain reservoir ($z>L$) denoted as D. Their chemical potentials are held at 0 and V_{DS}, respectively. If the complex band structure of the reservoirs is known, the respective Bloch eigenvectors $u_{\mathbf{G}}^{k_{Sp}}$ and $u_{\mathbf{G}}^{k_{Dp}}$ are also known. Here, p denotes the band index, running over $N_{\mathbf{G}}$ bands, which takes I for injected waves and R for reflected waves. Considering a 1D contact, we inject a wave with amplitude 1, $\psi^{k_{\mathrm{SI}}}(\mathbf{r})$, with a wavenumber k_{SI} in (sub-) band n at an energy $E=E^{(n)}(k_{\mathrm{SI}})$ from the source reservoir. The injected wave is partially reflected into the source contact as a wave $\psi^{k_{\mathrm{SR}}}(\mathbf{r})$ and partially transmitted into the drain contact as a wave $\psi^{k_{\mathrm{DR}}}(\mathbf{r})$. The wave in the region $z<0$, a superposition of the injected wave and the reflected wave, is then

$$\psi_l(\mathbf{r}) = \psi^{k_{\mathrm{SI}}}(\mathbf{r})+\psi^{k_{\mathrm{SR}}}(\mathbf{r}) = e^{ik_{\mathrm{SI}}z}\sum_{\mathbf{G}}u_{\mathbf{G}}^{k_{\mathrm{SI}}}e^{i\mathbf{G}\cdot\mathbf{r}} + \sum_{k_{\mathrm{SR}}}R_{k_{\mathrm{SR}}}(E)e^{ik_{\mathrm{SR}}z}\sum_{\mathbf{G}}u_{\mathbf{G}}^{k_{\mathrm{SR}}}e^{i\mathbf{G}\cdot\mathbf{r}}. \tag{B1}$$

Here, the quantities k_{SR} represent the (in general complex) wavevectors of the reflected waves. They satisfy the condition $E(k_{\mathrm{SR}})=E$. The quantities $R_{k_{\mathrm{SR}}}(E)$ are coefficients that remain to be determined. The wave in the region $z>L$ is just the transmitted wave

$$\psi^{k_{\mathrm{DR}}}(\mathbf{r}) = \sum_{k_{\mathrm{DR}}}T_{k_{\mathrm{DR}}}(E)e^{ik_{\mathrm{DR}}z}\sum_{\mathbf{G}}u_{\mathbf{G}}^{k_{\mathrm{DR}}}e^{i\mathbf{G}\cdot\mathbf{r}}, \tag{B2}$$

where k_{DR} are the wavevectors that satisfy the condition $E(k_{\mathrm{DR}})=E-eV_{\mathrm{DS}}$. The quantities $T_{k_{\mathrm{DR}}}(E)$ are also coefficients that remain to be determined. Comparing Eq. (B1) with the wavefunctions expressed using the envelope approach $\psi(\mathbf{r})=\sum_{\mathbf{G}}\phi_{\mathbf{G}}^{k_{\mathrm{SI}}}(z)e^{i\mathbf{G}\cdot\mathbf{r}}$ for the source reservoir injection, we have

$$\sum_{\mathbf{G}}\phi_{\mathbf{G}}^{k_{\mathrm{SI}}}(z)e^{i\mathbf{G}\cdot\mathbf{r}} = e^{ik_{\mathrm{SI}}z}\sum_{\mathbf{G}}u_{\mathbf{G}}^{k_{\mathrm{SI}}}e^{i\mathbf{G}\cdot\mathbf{r}} + \sum_{k_{\mathrm{SR}}}R_{k_{\mathrm{SR}}}(E)e^{ik_{\mathrm{SR}}z}\sum_{\mathbf{G}}u_{\mathbf{G}}^{k_{\mathrm{SR}}}e^{i\mathbf{G}\cdot\mathbf{r}}. \tag{B3}$$

Equating the coefficients of the expansion over $e^{i\mathbf{G}\cdot\mathbf{r}}$ term-by-term, we obtain

$$\phi_{\mathbf{G}}^{k_{\mathrm{SI}}}(z) = e^{ik_{\mathrm{SI}}z}u_{\mathbf{G}}^{k_{\mathrm{SI}}}+\sum_{k_{\mathrm{SR}}}R_{k_{\mathrm{SR}}}(E)e^{ik_{\mathrm{SR}}z}u_{\mathbf{G}}^{k_{\mathrm{SR}}}. \tag{B4}$$

Therefore, the wavefunction at $z_1=0$ is

$$\phi_{\mathbf{G}}^{k_{\mathrm{SI}}}(0) = u_{\mathbf{G}}^{k_{\mathrm{SI}}}+\sum_{k_{\mathrm{SR}}}R_{k_{\mathrm{SR}}}(E)u_{\mathbf{G}}^{k_{\mathrm{SR}}}, \tag{B5}$$

and the one at $z_0=-\Delta$ is

$$\phi_{\mathbf{G}}^{k_{\mathrm{SI}}}(-\Delta) = e^{-ik_{\mathrm{SI}}\Delta}u_{\mathbf{G}}^{k_{\mathrm{SI}}}+\sum_{k_{\mathrm{SR}}}R_{k_{\mathrm{SR}}}(E)e^{-ik_{\mathrm{SR}}\Delta}u_{\mathbf{G}}^{k_{\mathrm{SR}}}. \tag{B6}$$

Defining

$$r_{\mathbf{G}} = \sum_{k_{\mathrm{SR}}} R_{k_{\mathrm{SR}}}(E) u_{\mathbf{G}}^{k_{\mathrm{SR}}} \tag{B7}$$

so that $\phi_{\mathbf{G}}^{k_{\mathrm{SI}}}(0) = u_{\mathbf{G}}^{k_{\mathrm{SI}}} + r_{\mathbf{G}}$ and

$$\rho_{\mathbf{G}} = \sum_{k_{\mathrm{SR}}} R_{k_{\mathrm{SR}}}(E) e^{-ik_{\mathrm{SR}}\Delta} u_{\mathbf{G}}^{k_{\mathrm{SR}}}, \tag{B8}$$

so that $\phi_{\mathbf{G}}^{k_{\mathrm{SI}}}(-\Delta) = e^{-ik_{\mathrm{SI}}\Delta} u_{\mathbf{G}}^{k_{\mathrm{SI}}} + \rho_{\mathbf{G}}$, we have

$$R_{k_{\mathrm{SR}}}(E) = \sum_{\mathbf{G}} (u_{\mathbf{G}}^{k_{\mathrm{SR}}})^{-1} r_{\mathbf{G}}. \tag{B9}$$

Inserting Eq. (B9) into Eq. (B8), we obtain

$$\begin{aligned} \rho_{\mathbf{G}} &= \sum_{k_{\mathrm{SR}}} u_{\mathbf{G}}^{k_{\mathrm{SR}}} \sum_{\mathbf{G}'} (u_{\mathbf{G}'}^{k_{\mathrm{SR}}})^{-1} r_{\mathbf{G}'} e^{-ik_{\mathrm{SR}}\Delta} \\ &= \sum_{k_{\mathrm{SR}}} u_{\mathbf{G}}^{k_{\mathrm{SR}}} \sum_{\mathbf{G}'} (u_{\mathbf{G}'}^{k_{\mathrm{SR}}})^{-1} (\phi_{\mathbf{G}'}^{k_{\mathrm{SI}}}(0) - u_{\mathbf{G}'}^{k_{\mathrm{SI}}}) e^{-ik_{\mathrm{SR}}\Delta}. \end{aligned} \tag{B10}$$

The above expression permits us to express the wavefunction inside the contact $\phi_{\mathbf{G}}^{k_{\mathrm{SI}}}(-\Delta)$ in terms of the wavefunction in the device.

Considering Eq. (9) at $l = 1$ (i.e., $z_1 = 0$) for the energy $E = E^{(n)}(k_{\mathrm{SI}})$, we obtain the equation which relates the source reservoir to the device as

$$\begin{aligned} &-\frac{\hbar^2}{2m\Delta^2}\left[\phi_{\mathbf{G}}(z_2) + \phi_{\mathbf{G}}(z_0)\right] - i\frac{\hbar^2}{2m\Delta} G_z \left[\phi_{\mathbf{G}}(z_2) - \phi_{\mathbf{G}}(z_0)\right] \\ &+\left(\frac{\hbar^2}{m\Delta^2} - E\right)\phi_{\mathbf{G}}(z_1) + \sum_{\mathbf{G}'} W_{\mathbf{G},\mathbf{G}'}^{(1\mathrm{D})}(z_1)\phi_{\mathbf{G}'}(z_1) = 0. \end{aligned} \tag{B11}$$

Inserting $\phi_{\mathbf{G}}(z_0) = \phi_{\mathbf{G}}^{k_{\mathrm{SI}}}(-\Delta)$ into the equation above, the relation between the wavefunctions inside and outside the device is

$$\begin{aligned} &-\left(\frac{\hbar^2}{2m\Delta^2} + i\frac{\hbar^2}{2m\Delta} G_z\right)\phi_{\mathbf{G}}(z_2) + \left(\frac{\hbar^2}{m\Delta^2} - E\right)\phi_{\mathbf{G}}(z_1) \\ &+\sum_{\mathbf{G}'}\left(W_{\mathbf{G},\mathbf{G}'}^{(1\mathrm{D})}(z_1) + \Sigma_{\mathbf{G},\mathbf{G}'}^{(\mathrm{S})}\right)\phi_{\mathbf{G}'}(z_1) \\ &= \left(\frac{\hbar^2}{2m\Delta^2} - i\frac{\hbar^2}{2m\Delta} G_z\right)\cdot e^{-ik_{\mathrm{SI}}\Delta} u_{\mathbf{G}}^{k_{\mathrm{SI}}} + \sum_{\mathbf{G}'} \Sigma_{\mathbf{G},\mathbf{G}'}^{(\mathrm{S})} u_{\mathbf{G}'}^{k_{\mathrm{SI}}}, \end{aligned} \tag{B12}$$

where the term

$$\Sigma_{\mathbf{G},\mathbf{G}'}^{(\mathrm{S})} = -\left(\frac{\hbar^2}{2m\Delta^2} - i\frac{\hbar^2}{2m\Delta} G_z\right)\sum_{k_{\mathrm{SR}}} u_{\mathbf{G}}^{k_{\mathrm{SR}}} \left(u_{\mathbf{G}'}^{k_{\mathrm{SR}}}\right)^{-1} e^{-ik_{\mathrm{SR}}\Delta} \tag{B13}$$

can be viewed as the source-contact self-energy matrix. This tells us how the structure of the source reservoir affects the wavefunctions inside the device. This term is added to the block $\mathbf{D}^1$ in Eq. (10), so that the r.h.s term of Eq. (B12) becomes an inhomogeneous term representing the injection from the source reservoir, transforming the eigenvalue problem to be a linear system.

Comparing Eq. (B2) with the wavefunction expressed using the envelope approach $\psi(\mathbf{r}) = \sum_{\mathbf{G}} \phi_{\mathbf{G}}^{k_{\mathrm{SI}}}(z) e^{i\mathbf{G}\cdot\mathbf{r}}$ for the same source-reservoir injection, we have

$$\sum_{\mathbf{G}} \phi_{\mathbf{G}}^{k_{\mathrm{SI}}}(z) e^{i\mathbf{G}\cdot\mathbf{r}} = \sum_{k_{\mathrm{DR}}} T_{k_{\mathrm{DR}}}(E) e^{ik_{\mathrm{DR}}z} \cdot \sum_{\mathbf{G}} u_{\mathbf{G}}^{k_{\mathrm{DR}}} e^{i\mathbf{G}\cdot\mathbf{r}}. \tag{B14}$$

Comparing the coefficient of $e^{i\mathbf{G}\cdot\mathbf{r}}$ term-by-term, we have

$$\phi_{\mathbf{G}}^{k_{\mathrm{SI}}}(z) = \sum_{k_{\mathrm{DR}}} T_{k_{\mathrm{DR}}}(E) e^{ik_{\mathrm{DR}}z} \cdot u_{\mathbf{G}}^{k_{\mathrm{DR}}}. \tag{B15}$$

Thus, the wavefunction at $z_{N+1} = L + \Delta$ is

$$\phi_{\mathbf{G}}^{k_{\mathrm{SI}}}(z_{N+1}) = \sum_{k_{\mathrm{DR}}} T_{k_{\mathrm{DR}}}(E) e^{ik_{\mathrm{DR}}(L+\Delta)} u_{\mathbf{G}}^{k_{\mathrm{DR}}}, \tag{B16}$$

and at $z_N = L$ is

$$\phi_{\mathbf{G}}^{k_{\mathrm{SI}}}(z_N) = \sum_{k_{\mathrm{DR}}} T_{k_{\mathrm{DR}}}(E) e^{ik_{\mathrm{DR}}L} u_{\mathbf{G}}^{k_{\mathrm{DR}}}. \tag{B17}$$

Therefore, the coefficient $T_{k_{\mathrm{DR}}}(E)$ can be written as

$$T_{k_{\mathrm{DR}}}(E) = \sum_{\mathbf{G}} \phi_{\mathbf{G}}^{k_{\mathrm{SI}}}(z_N)(u_{\mathbf{G}}^{k_{\mathrm{DR}}})^{-1} e^{-ik_{\mathrm{DR}}L}. \tag{B18}$$

Inserting Eq. (B18) into Eq. (B16), the wavefunction inside the right contact is expressed using $\phi_{\mathbf{G}}^{k_{\mathrm{SI}}}(L)$ as

$$\phi_{\mathbf{G}}^{k_{\mathrm{SI}}}(z_{N+1}) = \sum_{k_{\mathrm{DR}}} u_{\mathbf{G}}^{k_{\mathrm{DR}}} \sum_{\mathbf{G}'} \phi_{\mathbf{G}'}^{k_{\mathrm{SI}}}(z_N)(u_{\mathbf{G}'}^{k_{\mathrm{DR}}})^{-1} e^{ik_{\mathrm{DR}}\Delta}. \tag{B19}$$

Considering Eq. (9) at $l = \mathrm{N}$ (i.e., $z_N = L$) for the energy $E = E^{(n)}(k_{\mathrm{SI}})$, the equation that relates the drain reservoir to the device is

$$\begin{aligned} &-\frac{\hbar^2}{2m\Delta^2}\left[\phi_{\mathbf{G}}(z_{N+1}) + \phi_{\mathbf{G}}(z_{N-1})\right] \\ &-i\frac{\hbar^2}{2m\Delta} G_z\left[\phi_{\mathbf{G}}(z_{N+1}) - \phi_{\mathbf{G}}(z_{N-1})\right] \\ &+\left(\frac{\hbar^2}{m\Delta^2} - E\right)\phi_{\mathbf{G}}(z_N) + \sum_{\mathbf{G}'} W_{\mathbf{G},\mathbf{G}'}^{(1\mathrm{D})}(z_N)\phi_{\mathbf{G}'}(z_N) = 0. \end{aligned} \tag{B20}$$

Inserting Eq. (B19) into the equation above, we have

$$\begin{aligned} &-\left(\frac{\hbar^2}{2m\Delta^2} - i\frac{\hbar^2}{2m\Delta} G_z\right)\phi_{\mathbf{G}}(z_{N-1}) + \left(\frac{\hbar^2}{m\Delta^2} - E\right)\phi_{\mathbf{G}}(z_N) \\ &+\sum_{\mathbf{G}'}\left(W_{\mathbf{G},\mathbf{G}'}^{(1\mathrm{D})}(z_N) + \Sigma_{\mathbf{G},\mathbf{G}'}^{(\mathrm{R})}\right)\phi_{\mathbf{G}'}(z_N) = 0, \end{aligned} \tag{B21}$$

where the term

$$\Sigma^{(\mathrm{R})}_{\mathbf{G},\mathbf{G}'} = -\left(\frac{\hbar^2}{2m\Delta^2} + i\frac{\hbar^2}{2m\Delta}G_z\right)\sum_{k_{\mathrm{DR}}} u^{k_{\mathrm{DR}}}_{\mathbf{G}}\left(u^{k_{\mathrm{DR}}}_{\mathbf{G}'}\right)^{-1} e^{ik_{\mathrm{DR}}\Delta} \tag{B22}$$

is the device/right-contact self-energy matrix. As we saw for the source reservoir, this matrix tells us how the structure of the drain reservoir affects the wavefunctions inside the device and is to be added to the block $\mathbf{D}^N$ in Eq. (10).

[1]J. Wang, E. Polizzi, and M. Lundstrom, J. Appl. Phys. **96**, 2192 (2004).
[2]J. Wang, A. Rahman, A. Ghosh, G. Klimeck, and M. Lundstrom, IEEE Trans. Electron Devices **52**, 1589 (2005).
[3]J.-L. van der Steen, D. Esseni, P. Palestri, L. Selmi, and R. J. Hueting, IEEE Trans. Electron Devices **54**, 1843 (2007).
[4]N. Neophytou, A. Paul, M. S. Lundstrom, and G. Klimeck, J. Comput. Electron. **7**, 363 (2008).
[5]B. Fu, "Quantum transport: From effective mass approximation to full band," Ph.D. dissertation (The University of Texas at Dallas, Richardson, TX, 2013).
[6]M. Luisier, M. Lundstrom, D. Antoniadis, and J. Bokor, IEEE Int. Electron Devices Meet. **2011**, 11.2.1–11.2.4.
[7]Y. Liu, N. Neophytou, T. Low, G. Klimeck, and M. Lundstrom, IEEE Trans. Electron Devices **55**, 866 (2008).
[8]S. Datta, Superlattices Microstruct. **28**, 253 (2000).
[9]H. J. Choi and J. Ihm, Phys. Rev. B **59**, 2267 (1999).
[10]A. Mayer, Carbon **42**, 2057 (2004).
[11]X.-W. Jiang, S.-S. Li, and L.-W. Wang, Solid-State Electron. **68**, 56 (2012).
[12]A. Garcia-Lekue, M. Vergniory, X. Jiang, and L. Wang, Prog. Surf. Sci. **90**, 292 (2015).
[13]S. O. Koswatta, S. Hasan, M. S. Lundstrom, M. Anantram, and D. E. Nikonov, IEEE Trans. Electron Devices **54**, 2339 (2007).
[14]Y. Yoon, D. E. Nikonov, and S. Salahuddin, Appl. Phys. Lett. **98**, 203503 (2011).
[15]M. Stettler *et al.*, in *2014 International Conference on Simulation of Semiconductor Processes and Devices (SISPAD)* (IEEE, 2014), pp. 13–16.
[16]M. Luisier and G. Klimeck, Device Research Conference **1**, 5 (2009).
[17]J. Guo, S. Datta, and M. Lundstrom, IEEE Trans. Electron Devices **51**, 172 (2004).
[18]M. Luisier and G. Klimeck, Phys. Rev. B **80**, 155430 (2009).
[19]Á. Szabó and M. Luisier, in *Proceedings of the European Solid-State Device Research Conference (ESSDERC)* (IEEE, 2013), pp. 77–80.
[20]G. Kresse and J. Furthmüller, Comput. Mater. Sci. **6**, 15 (1996).
[21]L. Yang, C.-H. Park, Y.-W. Son, M. L. Cohen, and S. G. Louie, Phys. Rev. Lett. **99**, 186801 (2007).
[22]M. Brandbyge, J.-L. Mozos, P. Ordejón, J. Taylor, and K. Stokbro, Phys. Rev. B **65**, 165401 (2002).
[23]J. Taylor, H. Guo, and J. Wang, Phys. Rev. B **63**, 245407 (2001).
[24]A. Sengupta and S. Mahapatra, J. Appl. Phys. **114**, 194513 (2013).
[25]M. Cohen and J. R. Chelikowsky, *Electronic Structure and Optical Properties of Semiconductors* (Springer Science and Business Media, 2012), Vol. 75.
[26]D. Esseni and P. Palestri, Phys. Rev. B **72**, 165342 (2005).
[27]X.-W. Jiang, S.-S. Li, J.-B. Xia, and L.-W. Wang, J. Appl. Phys. **109**, 054503 (2011).
[28]M. V. Fischetti, B. Fu, S. Narayanan, and J. Kim, "Semiclassical and quantum electronic transport in nanometer-scale structures: empirical pseudopotential band structure, Monte Carlo simulations and Pauli master equation," in *Nano-Electronic Devices: Semiclassical and Quantum Transport Modeling*, edited by D. Vasileska and Stephen M. Goodnick (Springer, New York, 2011), pp. 183–247.
[29]J. Fang, W. Vandenberghe, and M. Fischetti, in *2014 International Workshop on Computational Electronics (IWCE)* (IEEE, 2014), pp. 1–3.
[30]J. Fang, W. Vandenberghe, and M. Fischetti, in *TECHCON* (SRC, 2014), pp. 1–4.
[31]M. Burt, J. Phys.: Condens. Matter **11**, 53 (1999).
[32]W. Kohn and J. M. Luttinger, Phys. Rev. **98**, 915 (1955).
[33]C. S. Lent and D. J. Kirkner, J. Appl. Phys. **67**, 6353 (1990).
[34]Y.-C. Chang and J. Schulman, Phys. Rev. B **25**, 3975 (1982).
[35]S. Zhang, C.-Y. Yeh, and A. Zunger, Phys. Rev. B **48**, 11204 (1993).
[36]L. W. Wang and A. Zunger, J. Phys. Chem. **98**, 2158 (1994).
[37]T. Ando, A. B. Fowler, and F. Stern, Rev. Mod. Phys. **54**, 437 (1982).
[38]W. Pötz, J. Appl. Phys. **66**, 2458 (1989).
[39]W. R. Frensley, Rev. Mod. Phys. **62**, 745 (1990).
[40]M. Fischetti, Phys. Rev. B **59**, 4901 (1999).
[41]G. Breit and E. Wigner, Phys. Rev. **49**, 519 (1936).
[42]G. Lewicki and J. Maserjian, J. Appl. Phys. **46**, 3032 (1975).
[43]T. A. Davis, ACM Trans. Math. Software (TOMS) **30**, 196 (2004).

Pseudopotential-Based Electron Quantum Transport: Theoretical Formulation and Application to Nanometer-Scale Silicon Nanowire Transistors

Citation:

Fang, J., W. G. Vandenberghe, B. Fu, and M. V. Fischetti. 2016. "Pseudopotential-based electron quantum transport: Theoretical formulation and application to nanometer-scale silicon nanowire transistors." Journal of Applied Physics 119(3), doi:10.1063/1.4939963.